Electronic Supplementary Information

For

All-inorganic ferric wheel based on hexaniobate-anion linkages

Mark Baranov[†,a], Libi Polin[†,a], Nitai Leffler[a], Gregory Leitus[b], Alexander I. Shames[c] and Ira A. Weinstock[,a]*

[a]Department of Chemistry and the Ilse Katz Institute for Nanoscale Science & Technology, Ben-Gurion University of the Negev, Beer Sheva, 84105, Israel

[b]Chemical Research Support Unit, Weizmann Institute of Science, Rehovot 76100, Israel

[c]Department of Physics, Ben-Gurion University of the Negev, Beer Sheva 84105, Israel

† These authors have contributed equally to the work.

EXPERIMENTAL SECTION

Instruments and materials. All chemicals were of the reagent grade purity. Type I micropure standard water (18.2 Ω·cm), Lithium hydroxide (LiOH, 98%, solid, Sigma Aldrich); Iron (III) chloride ($FeCl_3$, yellow solid, Alfa Aesar Holland); Lithium perchlorate anhydrous ($LiClO_4$, crystalline, Holland Moran). $Li_8Nb_6O_{19}\cdot22H_2O$ was prepared using a published method.[1] We have used the lithium salt due to its low solubility, the salt slowly dissolves into the solution upon addition of Fe^{3+} and its subsequent complexation by hexaniobate, thus allowing us to kinetically regulate the reaction through the inherent solubility properties of the salt.

X-Ray diffraction analysis- The complex was mounted on a Rigaku XtalLAB Synergy single crystal x-ray diffractometer, which includes a Pilatus detector and a standard Cu $K\alpha$ x-ray radiation source ($\lambda = 1.51418$ Å). Unit cell dimensions, space group assignment, data reduction and finalization were done by using the CrysAlis PRO software package.[2] A total of 128352 reflections were collected, of which 31875 were used after merging by SHELXL[3] according to the crystal class and based on Friedel pair equivalency for structure solution. Numerical absorption correction based on gaussian integration over a multifaceted crystal model and empirical absorption correction was done using spherical harmonics.[4] The structure was solved in the orthorhombic *Pccn* space group (no. 56) by SHELXT[5] via intrinsic phasing and refined by SHELXL using a full-matrix least-squares. Due to solvent disorder the SQUEEZE command (solvent mask) was used for a volume of 8202 Å^3, for an equivalent of 246 e$^-$ per asymmetric unit, which is consistent with a presence of 32 H_2O molecules per unit formula (for a total of 88 H_2O solvent molecules, later confirmed by elemental analysis). Additionally, two Nb positions are disordered within the structure due to thermal motion, with partial occupancies of 26:74. CCDC deposition number: 2075364.

pH Measurements- pH values were measured using a Thermo SCIENTIFIC, ORION STAR A211 pH meter, or a EUTECH INSTRUMENTS, cyberscan pH 11 pH/ mv/ °C Meter. Prior to use, the pH meter was calibrated using standard reference solutions (pH 4.01, 7.00 and 10.01).

Elemental analysis - Elemental analysis of the metal content (Li, Nb and Fe) was performed using a SPECTRO ACROS ICP-OES analyzer calibrated using standard solutions of the respective elements. Elemental analysis of oxygen and hydrogen was performed using a Thermo Scientific Flash Smart OEA 2000 elemental analyzer, with water content determined directly as H_2O gas and the remaining O content determined using nickel coated carbon to quantitively yield CO while reducing the metal content.

FTIR spectroscopy- The FT-IR spectra were acquired using a Nicolet Impact 410 spectrophotometer (KBr pellets), analyzed with Omnic 7 software in transmission mode.

Magnetic susceptibility - Measurements were carried out using a MPMS3 (LOT-Quantum Design inc.) SQUID-magnetometer. Sample mass: 6.6 mg. Measurements were performed by VSM (vibrating sampling magnetometry) mode using peak amplitude 5mm; frequency 13 Hz; Averaging time 5 s. Chemical formula applied during calculations: $Li_6Nb_6Fe_1O_{27}$ (1 Fe^{3+} equimolar formula, molecular weight =1086.9128 g/mol). Pascal coefficients sum χ_0 = -1.942 10^{-4} $cm^3\,mol^{-1}$.

Electron paramagnetic resonance - Continuous wave X-band (9.4 GHz) EPR measurements were carried out using a Bruker EMX - 220 spectrometer (Bruker Scientific Israel Ltd., Rehovot, Israel) installed at the Ben-Gurion University of the Negev (Israel) and equipped with a 53150A frequency counter (Agilent Technologies Inc., Santa Clara, CA) and an Oxford Instruments ESR900 variable temperature accessory (Oxford Instruments plc, Tubney Woods, UK). EPR measurements were done within the temperature region $5\,K \leq T \leq 300\,K$. EPR data processing and fittings were carried out using WIN-EPR (Bruker), EasySpin,[6] and OriginLab (OriginLab Corporation, Northampton, MA) software packages.

Table S1. Crystal Data and Structure Refinement Details of 1

Crystal data	
Chemical Formula	$Li_{48}[(Nb_6O_{19})_8Fe_8(OH)_8]\cdot88H_2O$
M_r (g·mol^{-1})	9392.82
Crystal system, space group	Orthorhombic, *Pccn*
Temperature	100
Radiation type, λ (Å)	Cu K_α, 1.51418
a, b, c (Å)	22.5729 (6), 32.4190 (3), 43.4373 (5)
V (Å^3)	31787.0 (10)
μ (mm^{-1})	17.12
Z	4
ρ_{calcd} (g·cm^{-3})	1.957

Data collection	
Diffractometer	Rigaku Oxford Diffraction XtaLAB Synergy, Dualflex, Pilatus
Absorption correction	Gaussian, *CrysAlis PRO* 1.171.40.68a.{Rigaku, 2018 #22} Numerical absorption correction using a multifaceted crystal model based on gaussian integration. Empirical absorption correction using spherical harmonics, implemented in SCALE3 ABSPACK scaling algorithm.[4]
T_{min}, T_{max}	0.366, 1.000
No. of measured, independent and observed [$I > 2\sigma(I)$] reflections	128352, 31875, 24542
R_{int}	0.079
$(\sin\theta/\lambda)_{max}$ (Å^{-1})	0.625

Refinement	
$R[F^2 > 2\sigma(F^2)]$, $wR(F^2)$, S	0.077, 0.248, 1.09
No. of reflections	31875
No. of parameters	1449
$\Delta\rho_{max}$, $\Delta\rho_{min}$ (e· Å^{-3})	1.94, −1.66
Weighting scheme	$w = 1/[\sigma^2(F_o^2) + (0.1707P)^2 + 31.9223P]$ where $P = (F_o^2 + 2F_c^2)/3$

Symmetry codes: (i) x, y, z, (ii) ½ - x, y, ½ + z, (iii) x, ½ - y, ½ + z, (iv) ½ + x, ½ + y, -z, (v) -x, -y, -z, (vi) ½ + x, -y, ½ - z, (vii) -x, ½ + y, ½ - z, (viii) ½ - x, ½ - y, z

Table S2. Selected Bond Lengths (Å) for 1

Site 1	Site 2	Distance	Site 1	Site 2	Distance
Nb1	O64	2.053(6)	Nb9	O5	2.003(8)
Nb1	O63	1.940(7)	Nb9	O16	2.028(7)
Nb1	O73	1.920(6)	Nb9	O10	2.392(6)
Nb1	O71	2.070(6)	Nb9	O17	1.957(8)
Nb1	O62	1.814(6)	Nb9	O19	1.972(8)
Nb1	O70	2.335(6)	Nb9	O18	1.779(7)
Nb2	O6	2.040(7)	Nb10	O54	2.383(6)
Nb2	O10	2.395(7)	Nb10	O43	2.079(6)
Nb2	O9	2.026(7)	Nb10	O41	2.059(7)
Nb2	O46	1.972(8)	Nb10	O56	1.918(6)
Nb2	O19	1.964(7)	Nb10	O49	1.928(7)
Nb2	O7	1.757(8)	Nb10	O55	1.783(7)
Nb3	O39	2.164(10)	Nb11	O33	2.342(7)
Nb3	O38	1.705(10)	Nb11	O39	1.962(8)
Nb3	O35	1.953(10)	Nb11	O38	2.103(9)
Nb3	O32	2.444(13)	Nb11	O35	1.966(9)
Nb3	O36	1.617(10)	Nb11	O32	1.883(11)
Nb4	O54	2.407(6)	Nb11	O36	1.830(10)
Nb4	O53	2.007(7)	Nb12	O3	2.068(6)
Nb4	O50	1.996(6)	Nb12	O4	1.807(7)
Nb4	O47	1.995(6)	Nb12	O8	2.044(6)
Nb4	O80	1.981(6)	Nb12	O6	1.916(7)
Nb4	O52	1.797(7)	Nb12	O5	1.935(7)
Nb5	O13	2.033(8)	Nb12	O10	2.357(7)
Nb5	O12	1.755(8)	Fe1	O26	2.081(7)
Nb5	O17	1.976(7)	Fe1	O37	2.144(6)
Nb5	O46	1.962(8)	Fe1	O60	2.103(7)
Nb5	O11	2.016(8)	Fe1	O59	1.951(7)
Nb5	O10	2.395(7)	Fe1	O62	1.962(6)
Nb5	O13	2.033(8)	Fe1	O61	1.905(7)
Nb6	O54	2.328(5)	Fe2	O43	2.072(7)
Nb6	O43	2.083(6)	Fe2	O51	2.119(6)
Nb6	O51	2.048(7)	Fe2	O41	2.089(6)
Nb6	O47	1.940(6)	Fe2	O44	1.974(7)
Nb6	O45	1.930(6)	Fe2	O40	1.945(8)
Nb6	O44	1.779(6)	Fe2	O42	1.892(9)
Nb7	O73	2.003(6)	Fe3	O64	2.180(7)
Nb7	O34	2.004(7)	Fe3	O71	2.090(6)
Nb7	O72	1.986(8)	Fe3	O68	2.063(7)
Nb7	O70	2.418(6)	Fe3	O22	1.953(7)
Nb7	O79	1.950(7)	Fe3	O20	1.952(7)
Nb7	O74	1.780(7)	Fe3	O21	1.915(8)
Nb8	O54	2.341(6)	Fe4	O3	2.075(7)
Nb8	O51	2.057(6)	Fe4	O4	1.959(7)
Nb8	O53	1.940(6)	Fe4	O8	2.137(6)
Nb8	O58	1.922(6)	Fe4	O14	2.120(7)
Nb8	O41	2.061(6)	Fe4	O1	1.967(7)
Nb8	O59	1.818(7)	Fe4	O2	1.926(8)

Table S3. Selected Bond Angles (°) for 1
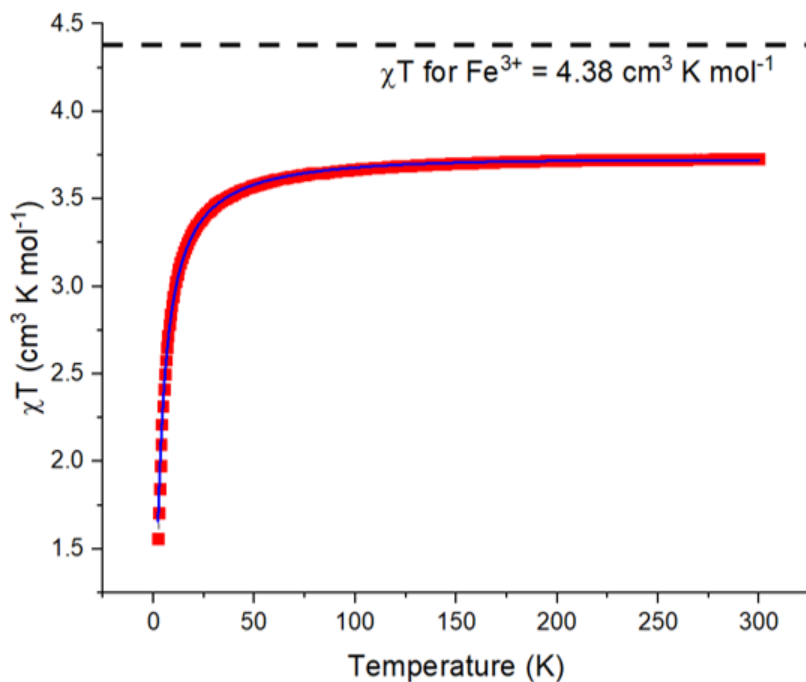
Site 1	Site 2	Site 3	Angle	Site 1	Site 2	Site 3	Angle
Nb1	O1	Nb13	114.7(3)	O11	Nb18	O9	91.7(3)
Nb1	O2	Nb9	110.9(3)	O9	Nb18	O8	89.2(3)
Nb1	O2	Fe4	99.3(3)	O9	Nb18	O14	155.9(3)
Nb9	O2	Fe4	99.2(3)	O9	Nb18	O10	79.5(3)
Nb2	O3	Fe1	100.0(2)	O20	Nb18	O8	102.6(3)
Nb2	O3	Nb35	110.7(5)	O20	Nb18	O14	99.8(3)
Nb4	O6	Nb3	89.4(3)	O20	Nb18	O10	177.0(3)
Nb4	O6	Nb6	92.7(2)	O20	Nb18	O11	100.9(3)
Nb4	O6	Nb7	93.2(3)	O20	Nb18	O9	103.5(3)
Nb4	O6	Nb8	91.0(3)	O75	Nb20	O54	78.1(2)
Nb4	O6	Nb11	179.0(4)	O75	Nb20	O50	89.4(3)
Nb6	O6	Nb3	88.7(2)	O75	Nb20	O45	153.6(3)
Nb6	O6	Nb7	91.8(3)	O75	Nb20	O49	87.4(3)
Nb7	O40	Fe3	98.5(3)	O45	Nb20	O54	75.7(2)
Fe1	O3	Nb35	101.5(4)	O45	Nb20	O49	84.3(3)
Fe2	O16	Nb33	157.1(10)	O50	Nb20	O54	78.3(3)
Fe2	O26	Nb31	96.9(6)	O50	Nb20	O45	87.6(3)
Fe2	O53	Nb20	97.3(3)	O50	Nb20	O49	154.8(3)
Fe4	O44	Nb12	100.2(3)	O72	Nb22	O63	88.2(3)
O1	Nb1	O2	90.6(2)	O72	Nb22	O66	153.7(3)
O1	Nb1	O17	79.0(2)	O72	Nb22	O70	78.2(3)
O2	Nb1	O17	77.0(2)	O23	Nb26	O26	89.6(3)
O38	Nb1	O17	177.8(3)	O23	Nb26	O37	156.0(3)
O38	Nb1	O55	100.5(3)	O23	Nb26	O33	79.7(3)
O38	Nb1	O56	101.8(3)	O23	Nb26	O38	92.5(3)
O55	Nb1	O2	78.5(2)	O26	Fe1	O37	76.5(3)
O55	Nb1	O17	77.3(2)	O26	Fe1	O60	76.1(3)
O56	Nb1	O55	88.9(3)	O60	Fe1	O37	76.1(3)
O7	Nb2	Nb12	134.1(3)	O59	Fe1	O26	162.8(3)
O7	Nb2	Nb18	134.9(3)	O59	Fe1	O37	87.7(3)
O7	Nb2	Nb9	134.8(3)	O59	Fe1	O60	93.7(3)
O7	Nb2	Nb5	135.3(3)	O59	Fe1	O62	93.1(3)
O7	Nb2	O6	102.5(4)	O62	Fe1	O26	94.6(3)
O7	Nb2	O10	179.1(4)	O62	Fe1	O37	92.9(3)
O7	Nb2	O9	103.2(3)	O62	Fe1	O60	166.9(3)
O7	Nb2	O46	103.9(4)	O61	Fe1	O26	95.9(3)
O7	Nb2	O19	103.0(4)	O61	Fe1	O37	167.3(3)
O5	Nb3	O6	77.4(2)	O61	Fe1	O60	92.3(3)
O43	Nb3	O6	77.8(3)	O61	Fe1	O59	98.3(3)
O47	Nb5	O13	100.7(5)	O61	Fe1	O62	97.9(3)
O47	Nb5	O25	106.9(6)	O16	Fe2	O26	93.7(3)
O74	Nb7	O73	102.9(3)	O16	Fe2	O53	88.5(3)
O74	Nb7	O34	102.7(3)	O16	Fe2	O57	163.5(3)
O74	Nb7	O72	102.9(3)	O26	Fe2	O53	76.4(3)
O11	Nb18	O8	155.6(3)	O28	Fe2	O16	96.8(3)
O11	Nb18	O14	90.1(3)	O28	Fe2	O26	91.6(3)
O11	Nb18	O10	79.2(3)	O28	Fe2	O38	97.9(3)

Table S4. Selected Bond Valence Sum Values for the Fe Atoms an
O Atoms Bound to Fe as OH Ligands in the Asymmetric Unit of 1
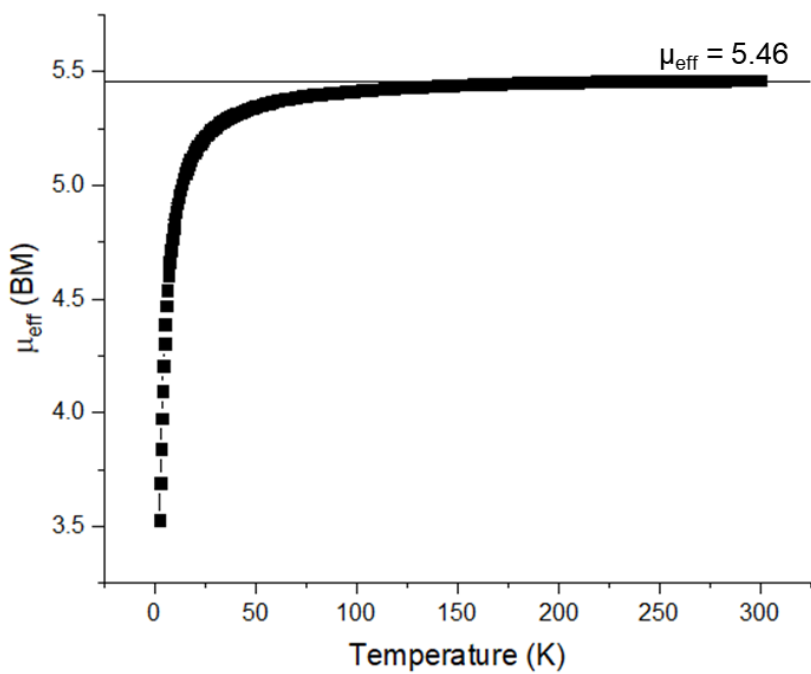
Atom	BVS value	Atom	BVS value
Fe1	3.06	O2	-0.7
Fe2	3.13	O21	-0.68
Fe3	3.06	O42	-0.71
Fe4	3.00	O61	-0.7

Table S5. ICP-OES and CHO Analysis Values Obtained for 1
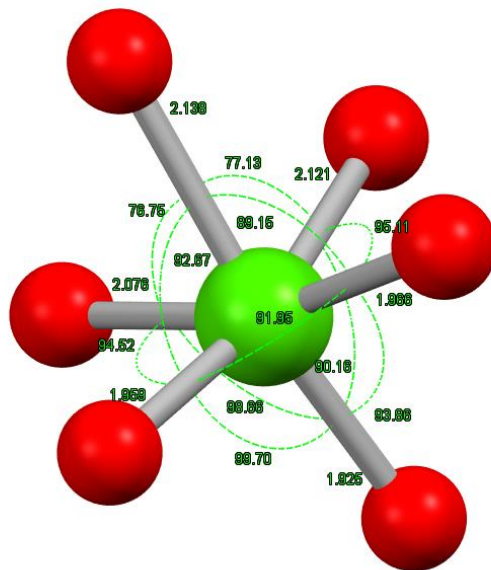
Atom type	Relative abundance compared to Fe
Fe	1
Nb	6.12
Li	5.97
O	31.44
H	22.97
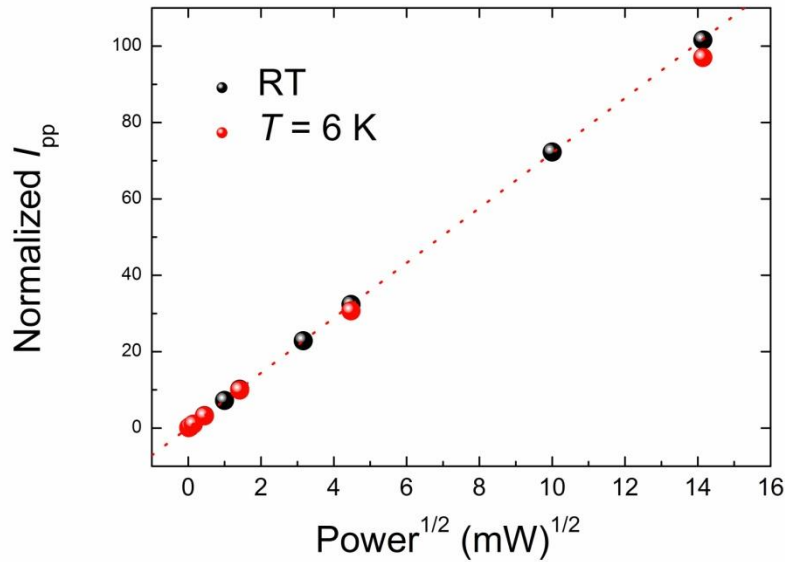
Figure S1. Magnetic susceptibility vs. temperature taken at H=5000 Oe is shown as $\chi T(T)$. The fitting by Curie-Weiss law is shown. The dash horizontal line show Curie constant values for non-interacting Fe^{3+} ions.
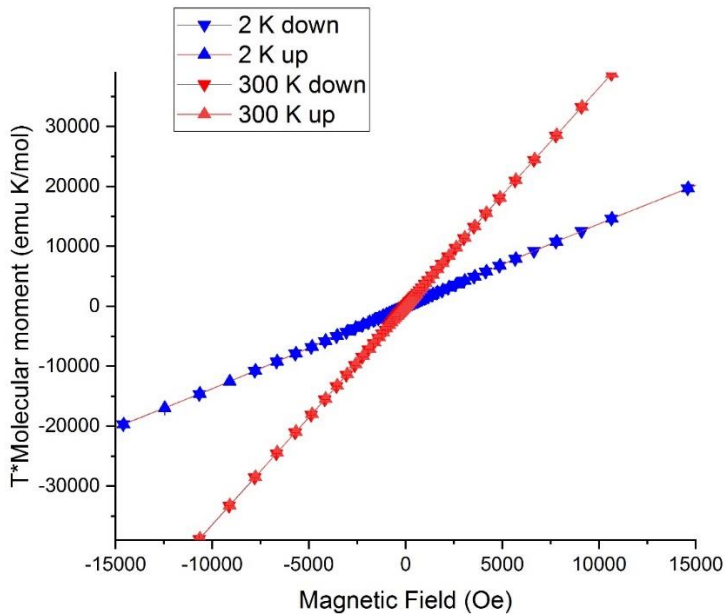
Figure S2. Effective magnetic moment curve, μ_{eff}, as a function of temperature for compound 1. The measured value of $\mu_{eff} = 5.46$ is lower than expected for non-interacting Fe^{3+} ions of $\mu = 5.92$, indicating exchange interactions between the Fe centers.
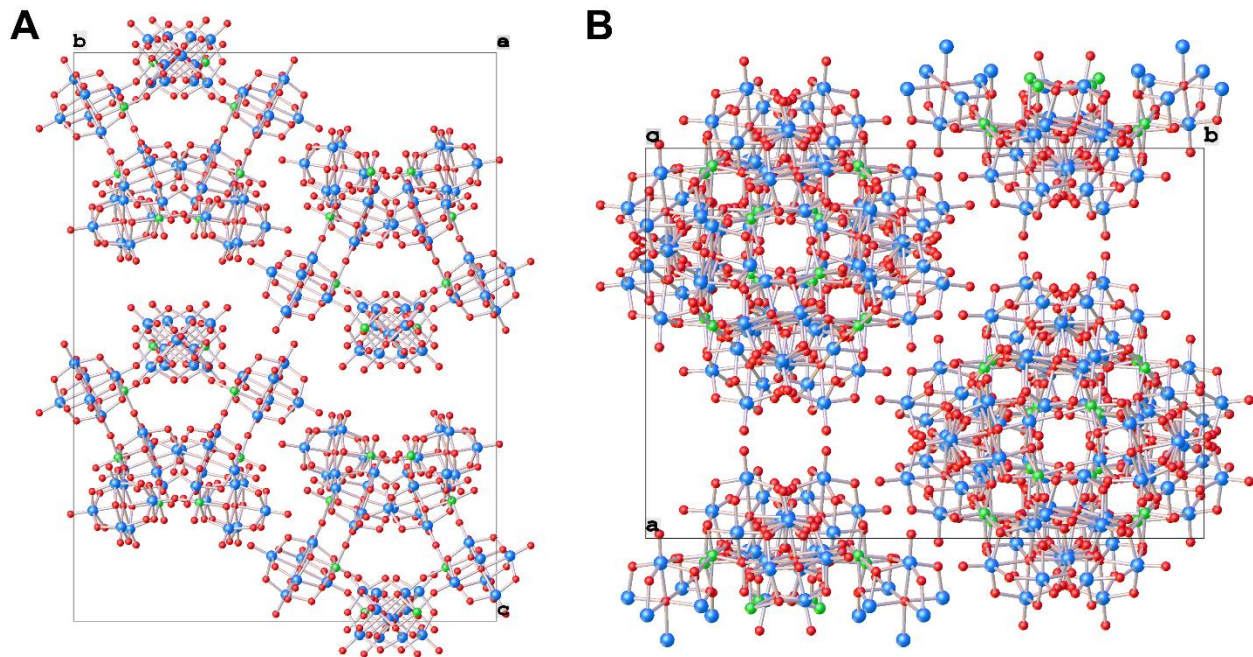

Figure S3. Distorted octahedral surrounding of one of the Fe-atom positions in the structure of **1**. The values of Fe-O distances and O-Fe-O angles are shown. The reason for the significant deviation from Curie's law lies in the strongly deformed octahedral oxygen environment of the Fe atoms.

Figure S4. Microwave power saturation of the intense $g_{iso} = 2.04$ line measured at two temperartures: black solid circles – room temperature (RT), red solid circles – $T = 6$K. Dashed red line represents best linear fit of the saturation curve obtained at RT.

**Figure S5.** The product of temperature and molar magnetic moment vs. magnetic field at T= 2 K and T=300 K. This figure shows that for fields less than 1 T, the field dependence of the magnetization can be considered linear over the entire temperature range. No hysteresis was found.

Figure S6. Crystal packing of **1**. A) View along [1 0 0], B) View along [0 0 1]. Solvent water and Li counter-cations are omitted for clarity.

References

1. M. Nyman, T. M. Anderson and P. P. Provencio, *Crystal Growth & Design*, 2009, **9**, 1036-1040.
2. Rigaku *CrysAlisPRO*, Yarnton, England, 2018.
3. G. Sheldrick, *Acta Crystallographica Section C*, 2015, **71**, 3-8.
4. *SCALE3 ABSPACK - An Oxford Diffraction program (1.0.4)*, Oxford Diffraction Ltd.: 2005.
5. G. Sheldrick, *Acta Crystallographica Section A*, 2015, **71**, 3-8.
6. S. Stoll and A. Schweiger, *Journal of Magnetic Resonance*, 2006, **178**, 42-55.